Electrochimica Acta 265 (2018) 569–576

Contents lists available at ScienceDirect

Electrochimica Acta

journal homepage: www.elsevier.com/locate/electacta

Understanding galvanic interactions between chalcopyrite and magnetite in acid medium to improve copper (Bio)Leaching

Albert Saavedra [a], J. Viridiana García-Meza [b], Eduardo Cortón [a], Ignacio González [c, *, 1]

[a] Biosensors and Bioanalysis Laboratory (LABB), Departamento de Química Biológica and IQUIBICEN-CONICET, Facultad de Ciencias Exactas y Naturales, Universidad de Buenos Aires (UBA), Ciudad Universitaria, Pabellón 2, Ciudad Autónoma de Buenos Aires, Argentina
[b] Geomicrobiología, Facultad de Ingeniería-Metalurgia, UASLP, Sierra Leona 550, Lomas 2, 78210 San Luis Potosí, Mexico
[c] Universidad Autónoma Metropolitana-Iztapalapa, Departamento de Química, Av. San Rafael Atlixco No. 186, Col. Vicentina, 09340, Ciudad de México, Mexico

ARTICLE INFO

Article history:
Received 8 November 2017
Received in revised form
23 January 2018
Accepted 26 January 2018
Available online 31 January 2018

Keywords:
Acid culture media
Chalcopyrite
Galvanic interactions
Magnetite
Copper extraction
Stripping voltammetry

ABSTRACT

Chalcopyrite is the main ore mineral used in industrial copper extraction. However, when passivation processes occur during hydrometallurgical treatment, a large percentage of the mineral being treated is not solubilized, so the copper recovery is limited. Galvanic interactions between semiconductor minerals are the basis of many strategies to achieve a more efficient process for increasing copper dissolution. These interactions concern generally two metallic sulfides. The present study describes a new galvanic interaction between chalcopyrite-magnetite ($CuFeS_2$-Fe_3O_4) in an acid microbial culture medium, used routinely in biomining processes. The electrochemical characterization of $CuFeS_2$, Fe_3O_4 and a mineral containing $CuFeS_2$-Fe_3O_4 is performed. Galvanic interactions are demonstrated by comparing Evans diagrams constructed from current transients obtained by imposing the potential pulses to each species studied. It is determined that $CuFeS_2$ and Fe_3O_4 fulfil the role of anode and cathode, respectively, in the behavior of the corresponding mineral. Stripping voltammetry is used to quantify electro-dissolved ions; the electrooxidation of $CuFeS_2$-Fe_3O_4 mineral in acid culture medium releases twice as many copper ions as pure chalcopyrite. This corroborates that the galvanic interactions prevent the formation of typical passivating components observed in chalcopyrite.

1. Introduction

Worldwide, 80% of copper is solubilized from copper sulfides and from copper- and iron-sulfide ores, such as chalcopyrite. Typically, copper is extracted by pyrometallurgical processes, but about 20% of copper worldwide is solubilized by (bio)hydrometallurgical processes (mainly low-grade oxides, carbonates and sulfides) [1]. Minerals composed of Cu-Fe-S show refractory properties, *i.e.,* they are not easily dissolved in aqueous solutions. In order to be dissolved at convenient (fast) rates, they need an oxidizing agent, usually ferric ions, which is incorporated into the leaching solutions. One of the main limitations of (bio)hydrometallurgical processes is the low solubilization of chalcopyrite, given that the dissolution of copper is typically lower than 35% [2].

The low dissolution of low-grade copper minerals may be due to several factors, one of them being the passivation phenomenon that occurs during the (bio)hydrometallurgical process. The oxidation of elemental sulfur is very slow, and this element is continuously accumulating on the mineral surface, forming a sulfur layer of difficult solubilization. Moreover, iron hydroxides, such as jarosite, precipitate and accumulate on the mineral surface too. Elemental sulfur and jarosite-like compounds are passivating agents that hinder further mineral dissolution, due to the diffusion barriers that these compounds represent [3–7].

A strategy to cope with passivation of minerals during hydrometallurgical processes is the use of sulfur-oxidizing bacteria that accelerate the oxidation of elemental sulfur [8]. Another strategy to improve the sulfide dissolution is the application of galvanic interactions [9–12] that occur when two minerals come into contact. During the galvanic interaction, the mineral with higher electrode potential acts as cathode and avoid its dissolution, while the mineral with lower potential acts as anode and is oxidized [13,14]. Galvanic interactions have been studied in aqueous leaching media,

* Corresponding author.
E-mail address: igm@xanum.uam.mx (I. González).
[1] ISE Member.

https://doi.org/10.1016/j.electacta.2018.01.169
0013-4686/

such as galena-sphalerite [15], pyrite-arsenopyrite [16] and in acid culture media, such as chalcopyrite-bornite [17], pyrite-bornite [18], among others.

Industrial processes have been developed based on the galvanic interactions present in minerals, *e.g.,* the GALVANOX™, which increases copper dissolution up to 98% and delays the passivation effect on chalcopyrite, depending on leaching time, acidification and pyrite addition [19,20].

One of the most studied galvanic interactions is the chalcopyrite-pyrite interaction in acid media, establishing a galvanic cell. In this system, chalcopyrite behaves as anode, and pyrite as cathode [21], increasing the chalcopyrite dissolution/corrosion significantly, and therefore increasing the copper release. The addition of bioleaching microorganisms to such a galvanic cell may increase the rate of copper dissolution even more [17,22–24].

Even though pyrite-chalcopyrite galvanic interaction is the most studied and the most industrially applied process, other minerals may exhibit this phenomenon as well: Magnetite-chalcopyrite association has been reported in different geological formations [25], but, to our knowledge, its electrochemical galvanic interaction has not yet been reported. Since magnetite is an oxide and chalcopyrite is a sulfide, their interaction might be a new alternative for application in the industrial recovery of copper.

In this study, an electrochemical characterization of the galvanic interaction of chalcopyrite-magnetite association under acidic conditions (pH 1.8) was performed using alternative techniques. This new information has been considered to improve the copper dissolution from chalcopyrite.

2. Experimental

2.1. Minerals

For this study, samples of three natural minerals were used: Chalcopyrite-magnetite ($CuFeS_2$-Fe_3O_4) and pure chalcopyrite and magnetite. Mineral identity and composition were then verified by X-ray diffraction patterns (XRD Rigaku 22002, $\Theta = 0.02$, 10–90°, using Cu-Kα radiation) and scanning electron microscopy (SEM, Philips XL30) coupled with an energy dispersive Si(Li) detector (EDAX DX4). Previous to XRD analysis, the samples were pulverized in an agate mortar. The $CuFeS_2$-Fe_3O_4 mineral was obtained from Tacna, Peru. Magnetite was observed to be dispersed within the crystals of chalcopyrite, and the XRD analysis indicated the presence of quartz as well (Fig. 1); thus, the composition of this mineral was: Chalcopyrite (67.05%), magnetite (0.56%) and quartz (32.39%). Quartz is not electrochemically active.

Magnetite (40.4%) containing quartz (38.41%), hematite (17.28%) and sphalerite (3.9%) was collected in Mexico. The chalcopyrite ($CuFeS_2$, 98.2% pure) was collected and selected from Charcas, San Luis Potosi (Mexico). Throughout the text and especially in the figures, the magnetite, chalcopyrite and chalcopyrite-magnetite minerals will be denominated M, C, and CM, respectively.

2.2. Electrochemical cell and microbial culture media

A typical 50-mL electrochemical cell with a three-electrode system was used. A modified 0 K microbial culture medium was used as electrolyte [26], supplemented with (g L^{-1}): KCl, 1; $MgSO_4 \cdot 7H_2O$, 0.2; $(NH_4)H_2PO_4$, 2.6. The pH was adjusted to 1.8 with 10 N H_2SO_4 solution (from a concentrated, 95% w/w H_2SO_4 solution). The electrochemical cell was stirred or not, depending on the experiment (see Section: "Electrochemical techniques"), using a magnetic stirrer, and the temperature was maintained at 30 °C using a thermostatic bath.

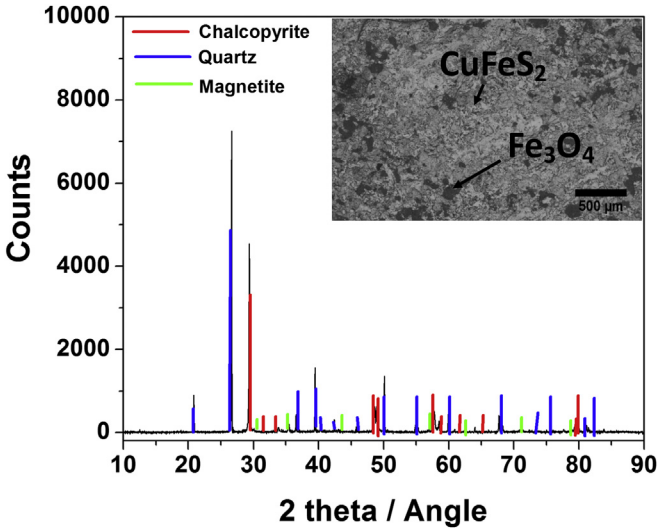

Fig. 1. XRD of $CuFeS_2$-Fe_3O_4 mineral. The inset shows a SEM image where magnetite is scattered among the crystals of chalcopyrite.

2.3. Electrodes

Massive electrodes of each of the three natural minerals (Section 2.1) were constructed and used as working electrodes (WEs). A massive sample of each mineral was cut in round shape and the electric contact was made with a copper wire attached to the mineral with silver paint. This assembly was encapsulated in epoxy resin and the exposed electrode area was *ca.* 1.0 cm^2. Before each experiment, the exposed surface was renewed by polishing with sandpaper (1200#). A graphite bar (Alfa Aesar, 99.999% purity) was used as a counter-electrode (CE). The reference electrode (RE) was $Hg/HgSO_4/K_2SO_{4(sat)}$ (SSE), (0.640 V/NHE) immersed in a Luggin capillary. All potential values reported in this study, unless otherwise stated, are referred to the normal hydrogen electrode (NHE).

2.4. Electrochemical techniques

For the electrochemical measurements, a potentiostat-galvanostat (Bio-Logic™, VMP3 model) equipped with data logger (EC-Lab *version* 9.98) and coupled to a 20 A, 20 V power supply (Bio-Logic™) was used. Different electrochemical techniques were performed to characterize the reactivity, galvanic interactions and the possible relevance of the methods proposed herein for the efficient dissolution of copper. These techniques are described below.

2.4.1. Open circuit potential and cyclic voltammetry

Open circuit potential (OCP) was measured by dipping the electrodes into the culture medium and monitored during 60 min, until achieving constant potential values. Cyclic voltammetry (CV) was conducted in both, anodic and cathodic directions, starting from the OCP, in a window potential of −0.46 to 1.04 V. For this study, a scan rate of $\upsilon = 20$ mV s^{-1} was used.

2.4.2. Chronoamperometry

Charge vs. applied-potential curves (Q vs. $E_{applied}$), as well as Evans diagrams of sampled current were constructed. Firstly, chronoamperometry curves were acquired at different potentials (between −0.46 to 1.04 V) during 30 s, covering the potential window in steps of 25 mV. After each experiment, the WE was mirror polished. The obtained chronoamperograms were used to

calculate the values of Q for each potential, based on the integration of the current curves *vs.* time ($Q = \int i\,dt$).

2.4.3. Evans diagram of sampled current

Evans diagrams were constructed by sampling the current (at different times: 1, 2, 3, 4 and 5 s) from the corresponding current transient obtained at different potentials. Evans diagrams were acquired by plotting log j_{sample} vs. *E*. This construction procedure is shown in Fig. 2.

The reaction rates for $CuFeS_2$-Fe_3O_4 and $CuFeS_2$ were estimated from Evans diagrams using the Faraday's equation. For this calculation, the following expression (Eq. (1)) was considered, where: I_{corr} is the corrosion current of the mineral, n is the number of transferred electrons, A is the exposed area, and F is the numerical value of the Faraday's constant [27].

$$r = \frac{I_{corr}}{nFA} \quad (1)$$

This was calculated from the current values obtained at the intersection of *i*/*E* curves. Corrosion currents ($CuFeS_2$-Fe_3O_4) were measured by drawing two Tafel straight lines in the anodic and cathodic direction, from the Evans diagram. Both the corrosion potential and current were obtained from the intersection point.

2.5. Electrochemical mineral dissolution analyzed by stripping voltammetry

To study the dissolution of the minerals, *E* was applied (1.015 V) for 60 s to $CuFeS_2$-Fe_3O_4 and $CuFeS_2$ minerals. The dissolution of copper and iron ions from the minerals in the electrolytic cell was evaluated by stripping voltammetry.

Copper was measured by anodic stripping, by means of a mercury film electrode (MFE) deposited on a vitreous carbon electrode disc (0.2 cm^2) used as WE. Aqueous samples from mineral dissolutions were quantified after adjusting their pH to 4.20, and after adding Hg^{2+} (final concentration of 2.10^{-5} M, final volume 50 mL); all this was done under vigorous magnetic agitation. The *E* utilized for deposition was −0.46 V (E_d) during 5 min. In this way, the mercury film and the analyte co-deposited forming an amalgam. At the end of the 5-min period, the agitation was suspended and after 30 s (quiet time), the stripping was done from −0.36–0.84 V. A differential pulse was used with $\upsilon = 5\ mV\ s^{-1}$, a pulse period of 0.10 s and a pulse amplitude of 10 mV. The electrochemical parameters used in the stripping analysis were previously optimized [28,29].

Iron was measured in similar conditions (volume, electrode material, agitation), but using a film of calomel, instead of mercury. The film was made in an electrochemical cell, in a solution 0.5 M HCl and 0.03 M Hg_2Cl_2. A potential of −0.46 V was applied during 3 min; after that, the activation was performed by a potential scan (from −0.36 to 1.64 V) at a rate of 5 mV. After activation, the electrode was transferred to another cell with a Britton-Robison buffer (0.04 M), adjusted to pH 4.20. Then, pyrogalol to a final concentration of 10^{-5} M was incorporated. The sample to be measured was then added, and a potential $E_d = -0.46$ V was applied during 5 min. At the end of the 5-min period, the agitation was suspended, and after 30 s (quiet time) the stripping was performed (from 0.34 to 0.84 V). A differential pulse was used with $\upsilon = 5\ mV\ s^{-1}$, a pulse period of 300 ms, and a pulse amplitude of 60 mV. This technique is a modification to that reported previously [30–32].

3. Results and discussion

3.1. Open circuit potential and cyclic voltammetry studies

The evolution of OCP is followed after immersion of the mineral electrode studied (Fe_3O_4, $CuFeS_2$ and $CuFeS_2$-Fe_3O_4), in 0 K culture medium (Fig. 3). Variations in OCP are attributed to the rearrangements of electric charges in the double layer formed at the mineral-solution interface and chemical interactions at this interface. The OCP reaches a stationary stage at approximately60 min of immersion, indicating a chemical modification of mineral surfaces provoked by the culture medium. The values of OCP are 0.495, 0.445 and 0.5 V, for Fe_3O_4, $CuFeS_2$ and $CuFeS_2$-Fe_3O_4 minerals, respectively. Throughout the text and especially in the figures, magnetite, chalcopyrite and chalcopyrite-magnetite minerals will be denominated M, C, and CM, respectively.

In order to characterize possible changes in the mineral surface (Fe_3O_4, $CuFeS_2$ and $CuFeS_2$-Fe_3O_4 are assayed) when the mineral is exposed to 0 K culture media, voltammetric studies are performed (Fig. 4).

When the scan potential is initiated in negative direction for Fe_3O_4 (Fig. 4A), two reduction processes take place: A wide

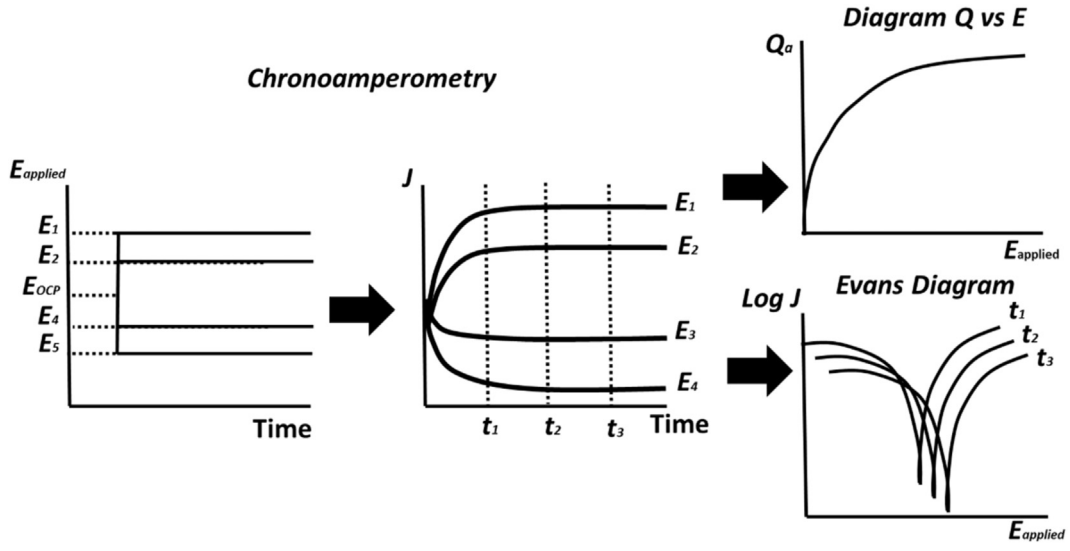

Fig. 2. Strategy used herein for characterization of galvanic systems and the procedure used for construction of Evans diagrams and charge curves.

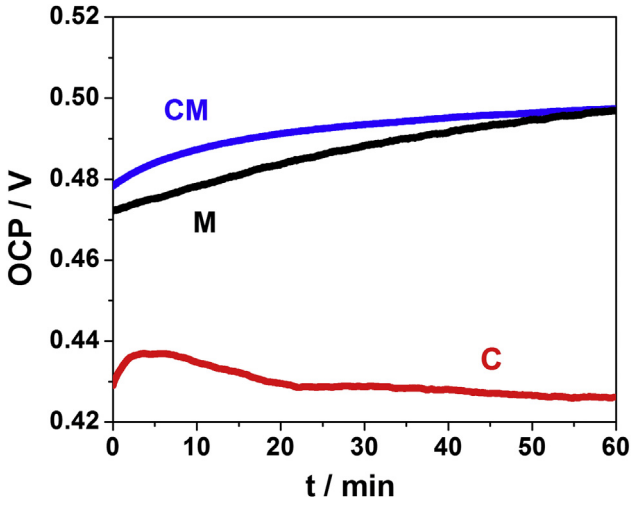

Fig. 3. Variation of the open circuit potential of minerals immersed in 0 K culture medium. M, Fe_3O_4; C, $CuFeS_2$; CM, $CuFeS_2$-Fe_3O_4.

reduction peak $C1_M$ appears at 0.18 V, while an additional reduction wave is detected from −0.2 V. Finally, when the scan potential is inverted, two oxidation peaks, $A1_M$ and $A2_M$, are observed at −0.08 and ~0.4 to 0.7 V, respectively. On the other hand, when the scan potential is initiated in positive direction (Fig. 4A), the voltammetry behavior is similar, but the current density ($\mu A\ cm^{-2}$) associated with reduction processes is higher. Current density is a useful way to express our results, given that our natural mineral samples do not have exactly the same area. The mineral geometric area is considered for current density calculation. This difference could be associated with mineral oxidation occurring in the positive scan direction ($A2_M$, with a scarcely observed current).

Rahner et al. [33], show that magnetite can be solubilized at 0.18 V *vs.* NHE (Eq. (2)), and the peak $C1_M$ could be thereby associated with this reaction. At higher potentials, magnetite can be oxidized to maghemite (γFe_2O_3 or $\gamma FeOOH$), Eq. (3) [34].

$$\left[Fe^{2+}Fe_2^{3+}\right]O_4(magnetite) + 8H^+ + 2e^- \rightarrow 3Fe^{2+} + 4H_2O \qquad (2)$$

$$3\left[Fe^{2+}Fe_2^{3+}\right]O_4(magnetite) \rightarrow 4\left[Fe_2^{3+}\right]O_4(maghemite) + Fe^{2+} + 2e^- \qquad (3)$$

When the scan potential is initiated in positive direction for $CuFeS_2$ (Fig. 4B), two important oxidation processes between ~0.54 and 0.74 V ($A1_C$), and another process beginning at ~0.83 V ($A2_C$) are observed. On the reverse scan, several cathodic processes take place. The first cathodic peak $C1_C$ is visible at 0.34 V, while the three cathodic peaks, $C2_C$, $C3_C$ and $C4_C$, appear at more negative potentials (at −0.04, −0.15 and −0.34 V, respectively). Finally, when the potential cycle is about to be completed, four anodic peaks ($A3_C$, $A4_C$, $A5_C$ and $A6_C$) are observed.

When the scan potential is initiated in negative direction (Fig. 4B), three cathodic reduction processes $C2_C$, $C3_C$ and $C4_C$ are observed. Upon reversing the sweep direction, six anodic peaks ($A3_C$, $A4_C$, $A5_C$, $A6_C$, $A7_C$ and $A2_C$) are seen in the same potential range and with a similar behavior in current density as the voltammogram obtained in positive direction (Fig. 4B). The chalcopyrite electrochemical behavior in culture media is complex and a deeper study is needed to establish the electrochemical transformation taking place. This study (electrochemical and Raman

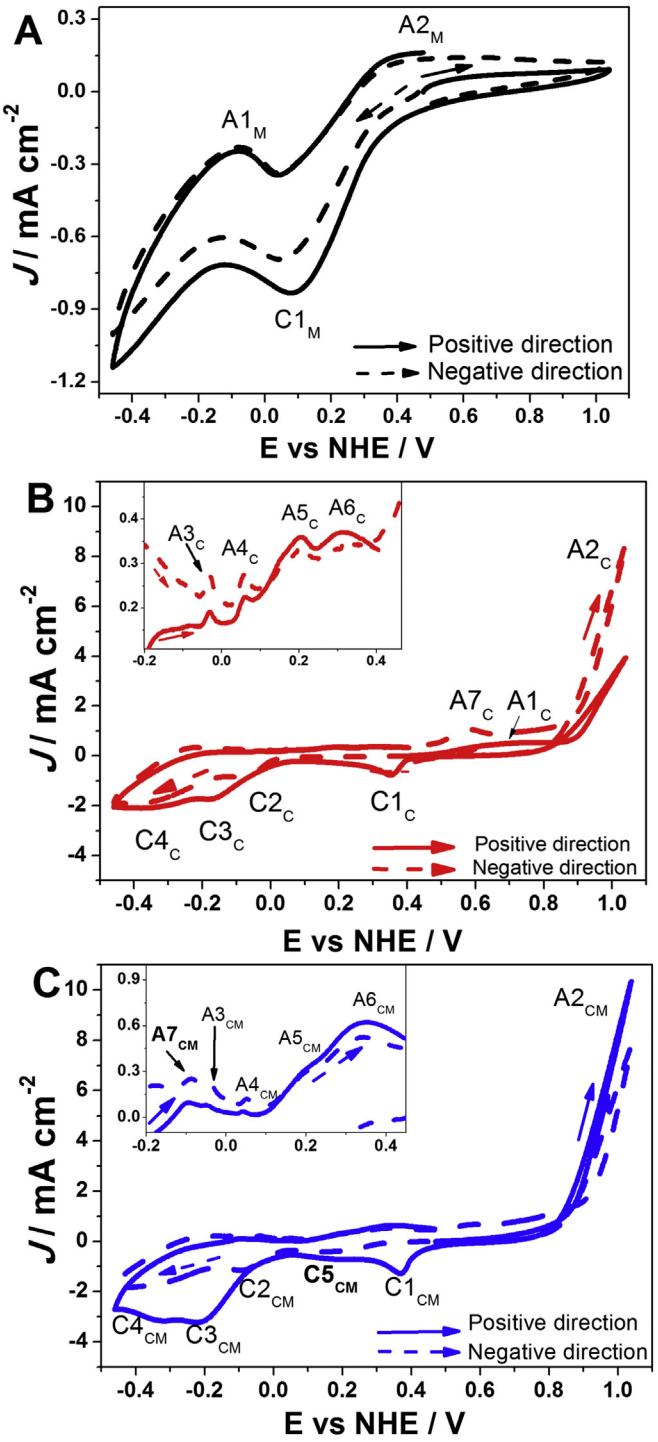

Fig. 4. Typical cyclic voltammograms ($v = 20\ mV\ s^{-1}$) obtained when the scan potential is initiated from OCP in positive (solid) and negative (dash) directions. A) Fe_3O_4, B) $CuFeS_2$, C) $CuFeS_2$-Fe_3O_4. The insets show detailed sections.

surface characterization) was previously performed by our research team [35], and the electrochemical reactions proposed in this manuscript were taken from this reference.

The peak $A1_C$ is associated with chalcopyrite oxidation in a culture medium similar to the one used in this work and identified with Eqs. (4) and (5) [35]:

$$CuFeS_{2(s)} \leftrightarrow Cu_{1-x}FeS_{2(s)} + xCu^{2+} + (2x)e^{-} \quad (4)$$

$$Cu_{1-x}FeS_{2(s)} + zCu^{2+}_{(l)} + yPO^{3-}_{4(l)} \leftrightarrow Cu_{1-x}Fe_{1-y}S_{2-z(s)} + zCuS_{(s)} + yFePO_{4(s)} + (3y-2z)e^{-} \quad (5)$$

The non-stoichiometric compounds, $Cu_{1-x}Fe_{1-y}S_{2-z(s)}$ and $FePO_{4(s)}$, formed in the initial chalcopyrite oxidation, are considered passivated compounds ($x = y$).

The peak $A2_C$ may correspond to chalcocite oxidation and, in its absence, to secondary sulfides, such as djurleite ($Cu_{1.92}S$), digenite ($Cu_{1.60}S$) and covellite (CuS), as shown in Eqs. (6)–(8) [17,36–38].

$$Cu_2S \rightarrow Cu_{1.92}S + 0.08Cu^{2+} + 0.16e^{-} \quad (6)$$

$$Cu_{1.92}S \rightarrow Cu_{1.6}S + 0.32Cu^{2+} + 0.64e^{-} \quad (7)$$

$$Cu_{1.6}S \rightarrow Cu + 0.06Cu^{2+} + 1.2e^{-} \quad (8)$$

The cathodic process $C1_C$ corresponds to reduction reactions (Eqs. (9)–(11) [39]) of the products formed at the interface in the direct potential scan, since it is not present when the scan is initiated in negative direction.

$$Fe^{3+} + e^{-} \rightarrow Fe^{2+} \quad (9)$$

$$Cu^{2+} + S^{0} + 2e^{-} \rightarrow CuS \quad (10)$$

$$Cu^{2+} + 2e^{-} \rightarrow Cu^{0} \quad (11)$$

The processes $C2_C$, $C3_C$ and $C4_C$, are associated with chalcopyrite reduction to secondary sulfide species, such as talnakhite ($Cu_9Fe_8S_{16}$), bornite (Cu_5FeS_4) and chalcocite (Cu_2S), which correspond to Eqs. (12)–(14) [17,36–40].

$$9CuFeS_2 + 4H^{+} + 2e^{-} \rightarrow Cu_9Fe_8S_{16} + 2H_2S + Fe^{2+} \quad (12)$$

$$5CuFeS_2 + 12H^{+} + 4e^{-} \rightarrow Cu_5FeS_4 + 6H_2S + 4Fe^{2+} \quad (13)$$

$$CuFeS_2 + 3Cu^{2+} + 4e^{-} \rightarrow 2Cu_2S + Fe^{2+} \quad (14)$$

The peaks $A3_C$ and $A4_C$ exhibit an activation behavior showing that metal copper is oxidized to chalcocite according to Eq. (15). When the potential is continued in forward scanning, anode oxidation peaks $A5_C$ and $A6_C$, which represent the oxidation of hydrogen sulfide to elemental sulfur, prove to be based on the reaction of Eq. (16) [36].

$$2Cu^{0} + H_2S \rightarrow Cu_2S + 2H^{+} + 2e^{-} \quad (15)$$

$$H_2S \rightarrow S^{0} + 2H^{+} + 2e^{-} \quad (16)$$

The peak $A7_C$ could be attributed to chalcocite oxidation forming a phase related to covellite (CuS) [41].

The voltammetric behavior of $CuFeS_2$-Fe_3O_4 mineral (Fig. 4C) is also complex and similar to that of chalcopyrite (Fig. 4B), displaying specific variations, mainly concerning the oxidation process.

Since OCP is different for each mineral, the overpotential study allows a better energetic comparison than the nominal OCP value. In order to show these variations, the current density *vs* overpotential (E-OCP) curves are constructed (Fig. 5), from voltammetric data (Fig. 4), for the studied minerals regarding the oxidation process.

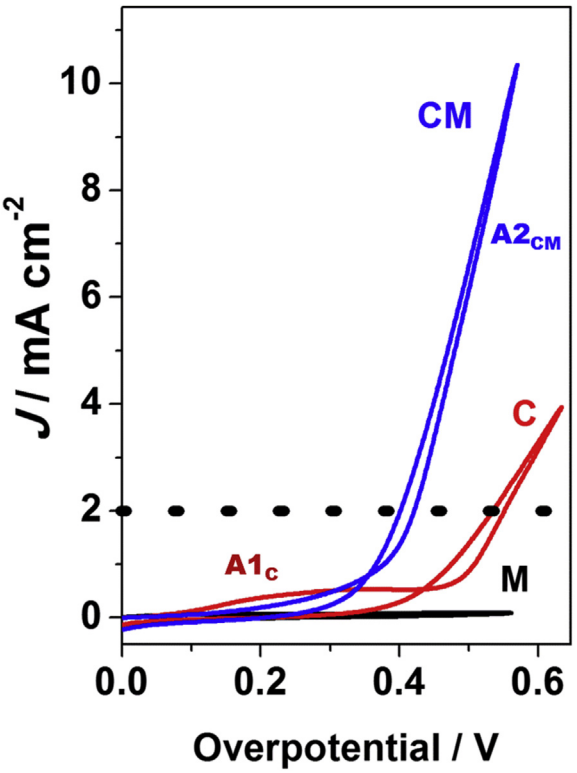

Fig. 5. Polarization curves constructed from data presented in Fig. 4. M, Fe_3O_4; C, $CuFeS_2$; CM, $CuFeS_2$-Fe_3O_4.

The chalcopyrite oxidation process associated with passive compounds formation ($A1_C$ peak, Fig. 5C) disappears in the presence of Fe_3O_4 (Fig. 5), provoking an increase in chalcopyrite oxidation process. The current associated with chalcopyrite transformation to easily oxidized copper compounds (reaction 5, 6 and 7) shows a significant increase ($A2_{CM}$ in Fig. 5CM), related to the fact that the overpotential for this oxidation is less positive than that required for chalcopyrite as a single mineral (Fig. 5C). In order to establish a quantitative measurement of this phenomenon, the overpotential necessary to achieve a chalcopyrite oxidation rate of 2 mA cm^{-2} is determined; however, even though the pure $CuFeS_2$ requires an overpotential of 0.55 V, the presence of Fe_3O_4 requires only 0.42 V (Fig. 5 dashed line).

This behavior is associated with the galvanic interaction between chalcopyrite and magnetite, in which the rest potential of the latter is more positive than that of the former, thus favoring the chalcopyrite oxidation.

Moreover, the voltammetric curves for $CuFeS_2$-Fe_3O_4 mineral (Fig. 4C) show additional peaks of $CuFeS_2$: a cathodic peak scarcely visible at 0.18 V and an oxidation peak ($A7_{CM}$), at 0.08 V. These peaks are related to the magnetite transformation (Fig. 4A).

The increase in mineral reactivity may be related to an increase in mineral solubilization [38]. The result obtained allows identifying anodic and cathodic processes of Fe_3O_4, present in the mixed $CuFeS_2$-Fe_3O_4 mineral. These processes are directly related to the increase in reactivity of the mixed mineral.

3.2. Potentiostatic studies

To avoid the competition between the velocity of energetic modification (potential scan rate) and velocity of electrochemical reaction at a specific potential (occurring during the linear sweep

voltammetry (LSV) [42]), in this work different potential pulses, within the potential range of −0.44 to 1.04 V, are applied to electrode surfaces. Typical current transients are obtained for $CuFeS_2$ by applying different potentials in the interval described (results not shown). All these kinetic behaviors could be associated with the formation of different secondary phases as a function of the applied potential.

Fig. 6 shows charge as a function of applied potential curves (Q *vs* overpotential), from all the minerals studied here (Fe_3O_4, $CuFeS_2$ and $CuFeS_2$-Fe_3O_4). To construct these curves, the total charge of oxidation process is evaluated when pulse potential is applied during 30 s. The imposed potential is represented as overpotential (E-OCP).

At higher overpotentials, the charge curves confirm the presence of galvanic interactions since the presence of magnetite significantly increases the charge associated with chalcopyrite oxidation. Furthermore, in the case of $CuFeS_2$-Fe_3O_4 at lower overpotentials, the stationary state obtained with potentitostatic studies allows detection of non-stoichiometric phases at $CuFeS_2$-Fe_3O_4 interface. These phases are not detected in the voltammetric characterization (Fig. 4), since the time constant (perturbation/response) in this technique is higher than that of potentiostatic techniques. In other conditions, our group has reported the formation of these phases over chalcopyrite samples [43]. However, the galvanic effect of magnetite always improves the chalcopyrite oxidation, because the overpotential at which these phases are formed is less positive and the associated charge is higher than those required for pure chalcopyrite.

The voltammetric and potentiostatic characterization of different minerals confirms that the presence of magnetite in the naturally mixed $CuFeS_2$-Fe_3O_4 mineral improves chalcopyrite oxidation due to galvanic interactions, in which chalcopyrite takes the role of anode (oxidation) and magnetite takes the role of cathode. This behavior is confirmed using Evans diagrams [42]. The Evans diagrams in this study are constructed from the corresponding current transients, where the current is sampled at different times (see Fig. 2 for the strategy used). Fig. 7 shows a typical Evans diagram that includes the oxidation polarization curve of chalcopyrite and reduction polarization curve of magnetite. The corrosion potential and current (mineral dissolution) are

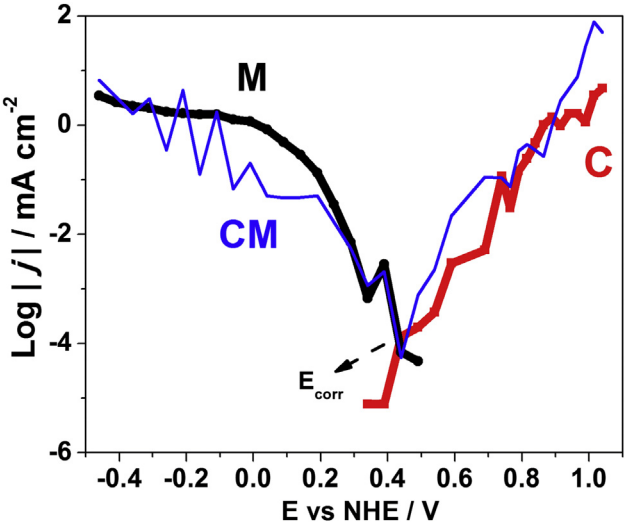

Fig. 7. Evans diagrams constructed from the corresponding potentiostatic current transients; the current is sampled at 5 s. M, Fe_3O_4; C, $CuFeS_2$; CM, $CuFeS_2$-Fe_3O_4. The corrosion potential (E_{corr}) is indicated.

obtained from the intersection of two straight lines traced on the anodic and cathodic branches of the Evans diagram.

The corrosion potential (E_{corr}) thus obtained is 0.45 V, equal to OCP obtained for naturally mixed $CuFeS_2$-Fe_3O_4 mineral (Fig. 3). In addition, the polarization curve of the mixed mineral is similar in both the anodic and cathodic branches of the Evans diagram, which confirms that Fe_3O_4 acts as cathode and $CuFeS_2$ as anode in galvanic interaction of $CuFeS_2$-Fe_3O_4 mineral. On the other hand, corrosion current density obtained from this diagram is 31.71 $\mu A\,cm^{-2}$, which corresponds to a corrosion rate of $3.30 \times 10^{-9}\,mol\,cm^{-2}\,s^{-1}$. This observed rate is small, so there is practically no leaching detected. Therefore, for any practical use the addition of a biological or chemical mediator will be necessary to increase the rate of mineral dissolution.

3.3. Solubilization of iron and copper from $CuFeS_2$ and $CuFeS_2$-Fe_3O_4

In order to confirm higher dissolution of chalcopyrite in the presence of magnetite, the oxidation of both minerals is performed

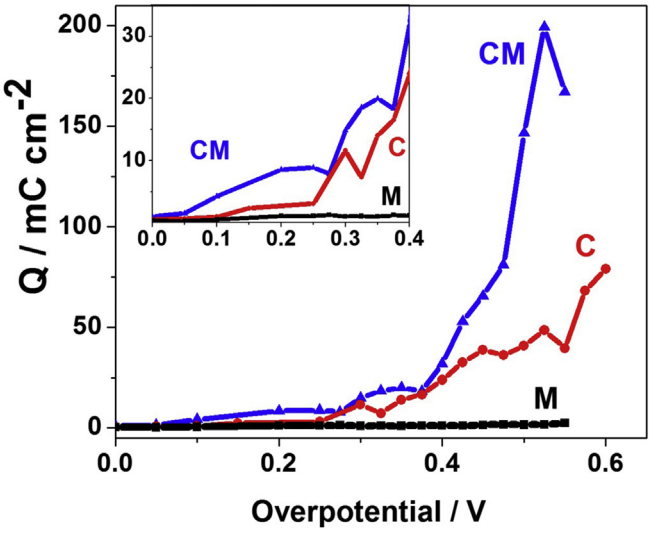

Fig. 6. Polarization curves constructed from the total charge (Q) involved in the current transients when different potentials are applied for 30 s. M, Fe_3O_4; C, $CuFeS_2$; CM, $CuFeS_2$-Fe_3O_4.

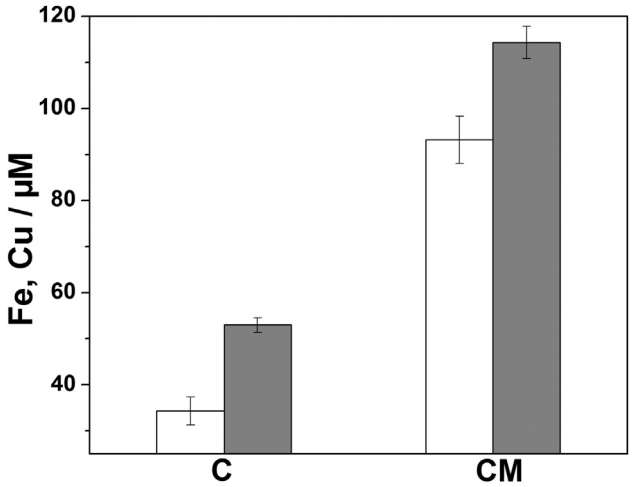

Fig. 8. Quantification of Fe (white) and Cu (gray) dissolved after 30 s at 1.025 V. C, $CuFeS_2$; CM, $CuFeS_2$-Fe_3O_4.

at 1.025 V during 30 s; this potential corresponds to a high reactivity zone. The copper and iron ions produced during the electrochemical oxidation are evaluated in the electrolytic solution. This evaluation represents a challenge because of the low concentration of these ions. The ions are quantified by means of electrochemical stripping analysis (see experimental section).

For the potential applied at 1.025 V (Fig. 8), $CuFeS_2$-Fe_3O_4 shows double and triple ions dissolved for Cu and Fe, respectively, compared to those dissolved for $CuFeS_2$, suggesting that the galvanic interaction strongly accelerates the mineral solubilization.

The ratios of solubilized Cu/Fe here obtained are 1.22 and 1.54 for $CuFeS_2$-Fe_3O_4 and $CuFeS_2$, respectively. That means that Cu concentrations are higher than Fe in both conditions, corresponding to a typical short-term chalcopyrite solubilization process [44–48], where free cations represent only 1% as $FeSO_{4(aq)}$ or $CuSO_{4(aq)}$. As leaching progresses, Fe concentration becomes more relevant, so the expected ratios are lower than 1 [45].

4. Conclusions

In this study, the galvanic interactions between two semiconductor minerals ($CuFeS_2$ and Fe_3O_4) naturally occurring in some ores is presented for the first time. We describe here an interesting galvanic pair ($CuFeS_2$-Fe_3O_4) that could be useful in copper leaching processes, given the relevant increase obtained in copper solubilization when compared to pure chalcopyrite.

The electrochemical characterization of $CuFeS_2$, Fe_3O_4 and a mineral containing $CuFeS_2$-Fe_3O_4 is performed in an acid culture medium, which is regularly used in biohydrometallurgical, industrial processes. This study shows that, in a natural mixed mineral, $CuFeS_2$ and Fe_3O_4 behave as an anode and a cathode, respectively, provoking an increase in chalcopyrite reactivity and preventing the formation of a passive layer commonly formed during the chalcopyrite oxidation. These results are confirmed by stripping analysis of copper and iron ions solubilized from electrochemical oxidation of $CuFeS_2$-Fe_3O_4 and $CuFeS_2$ minerals.

The results presented herein open new possibilities in the search of new, faster and economically viable processes in Cu mining. Moreover, these results can be extended to other sulfide/magnetite pairs of natural or manmade minerals. Preventing or delaying the formation of a passive layer over low-grade minerals can notably improve the efficiency and recovery of economically sound metals.

Acknowledgements

We want to acknowledge CONICET and UNU-BIOLAC for A Saavedra scholarship doctoral and internship respectively. Rosa Linda Tovar for DRX analyses; Erasmo Mata-Martínez for mineral section preparation.

References

[1] T. Norgate, S. Jahanshahi, Low grade ores – smelt, leach or concentrate? Miner. Eng. 23 (2010) 65–73.
[2] N. Pradhan, K.C. Nathsarma, K. Srinivasa Rao, L.B. Sukla, B.K. Mishra, Heap bioleaching of chalcopyrite: a review, Miner. Eng. 21 (2008) 355–365.
[3] C. Klauber, A. Parker, W. van Bronswijk, H. Watling, Sulphur speciation of leached chalcopyrite surfaces as determined by X-ray photoelectron spectroscopy, Int. J. Miner. Process. 62 (2001) 65–94.
[4] C. Klauber, A critical review of the surface chemistry of acidic ferric sulphate dissolution of chalcopyrite with regards to hindered dissolution, Int. J. Miner. Process. 86 (2008) 1–17.
[5] L.M. Cathles, J.A. Apps, A model of the dump leaching process that incorporates oxygen balance, heat balance, and air convection, Metall. Trans. B 6 (1975) 617–624.
[6] G. Debernardi, C. Carlesi, Chemical-electrochemical approaches to the study passivation of chalcopyrite, Miner. Process. Extr. Metall. Rev. 34 (2013) 10–41.
[7] K. Fu, H. Lin, X. Mo, H. Wang, H. Wen, Z. Wen, Comparative study on the passivation layers of copper sulphide minerals during bioleaching, Int. J. Miner. Metall. Mater. 19 (2012) 886–892.
[8] H. Pan, H. Yang, L. Tong, C. Zhong, Y. Zhao, Control method of chalcopyrite passivation in bioleaching, Trans. Nonferrous Metals Soc. China 22 (2012) 2255–2260.
[9] F.E. los Santos, R.E. Rivera-Santillán, M. Talavera-Ortega, F. Bautista, Catalytic and galvanic effects of pyrite on ferric leaching of sphalerite, Hydrometallurgy 163 (2016) 167–175.
[10] P.R. Holmes, F.K. Crundwell, Kinetic aspects of galvanic interactions between minerals during dissolution, Hydrometallurgy 39 (1995) 353–375.
[11] P.K. Abraitis, R.A.D. Pattrick, G.H. Kelsall, D.J. Vaughan, Acid leaching and dissolution of major sulphide ore minerals: processes and galvanic effects in complex systems, Miner. Mag. 68 (2004) 343–351.
[12] S.R. Rao, J.A. Finch, Galvanic interaction studies on sulphide minerals, Can. Metall. Q. 27 (1988) 253–259.
[13] T. Das, S. Ayyappan, G.R. Chaudhury, Factors affecting bioleaching kinetics of sulfide ores using acidophilic micro-organisms, Biometals 12 (1999) 1–10.
[14] I. Suzuki, Microbial leaching of metals from sulfide minerals, Biotechnol. Adv. 19 (2001) 119–132.
[15] G. Urbano, A.M. Meléndez, V.E. Reyes, M.A. Veloz, I. González, Galvanic interactions between galena–sphalerite and their reactivity, Int. J. Miner. Process. 82 (2007) 148–155.
[16] G. Urbano, V.E. Reyes, M.A. Veloz, I. González, Pyrite–arsenopyrite galvanic interaction and electrochemical reactivity, J. Phys. Chem. C 112 (2008) 10453–10461.
[17] J. Wang, L. Tao, H. Zhao, M. Hu, X. Zheng, H. Peng, X. Gan, W. Xiao, P. Cao, W. Qin, G. Qiu, D. Wang, Cooperative effect of chalcopyrite and bornite interactions during bioleaching by mixed moderately thermophilic culture, Miner. Eng. 95 (2016) 116–123.
[18] H. Zhao, J. Wang, X. Gan, X. Zheng, L. Tao, M. Hu, Y. Li, W. Qin, G. Qiu, Effects of pyrite and bornite on bioleaching of two different types of chalcopyrite in the presence of *Leptospirillum ferriphilum*, Bioresour. Technol. 194 (2015) 28–35.
[19] G. Nazari, D.G. Dixon, D.B. Dreisinger, Enhancing the kinetics of chalcopyrite leaching in the Galvanox™ process, Hydrometallurgy 105 (2011) 251–258.
[20] D.G. Dixon, D.D. Mayne, K.G. Baxter, Galvanox™ – a novel galvanically-assisted atmospheric leaching technology for copper concentrates, Can. Metall. Q. 47 (2008) 327–336.
[21] Z. Ekmekçi, H. Demirel, Effects of galvanic interaction on collector less flotation behaviour of chalcopyrite and pyrite, Int. J. Miner. Process. 52 (1997) 31–48.
[22] A.P. Mehta, L.E. Murr, Fundamental studies of the contribution of galvanic interaction to acid-bacterial leaching of mixed metal sulfides, Hydrometallurgy 9 (1983) 235–256.
[23] V.K. Berry, L.E. Murr, J.B. Hiskey, Galvanic interaction between chalcopyrite and pyrite during bacterial leaching of low-grade waste, Hydrometallurgy 3 (1978) 309–326.
[24] A.P. Mehta, L.E. Murr, Kinetic study of sulfide leaching by galvanic interaction between chalcopyrite, pyrite, and sphalerite in the presence of *T. ferrooxidans* (30°C) and a thermophilic microorganism (55°C), Biotechnol. Bioeng. 24 (1982) 919–940.
[25] S. Makvandi, G. Beaudoin, B.M. McClenaghan, D. Layton-Matthews, The surface texture and morphology of magnetite from the Izok Lake volcanogenic massive sulfide deposit and local glacial sediments, Nunavut, Canada: application to mineral exploration, J. Geochem. Explor. 150 (2015) 84–103.
[26] T.W. Kim, C.J. Kim, Y.K. Chang, H.W. Ryu, K.S. Cho, Development of an optimal medium for continuous ferrous iron oxidation by immobilized *Acidothiobacillus ferrooxidans* cells, Biotechnol. Prog. 18 (2002) 752–759.
[27] A.J. Bard, L.R. Faulkner, Electrochemical Methods: Fundamentals and Applications, Wiley, New York, 1980.
[28] J.L. Nava, I. Gonzalez, D. Nava, Electrochemical study of a flotation zinc concentrate in sulfuric acid: galvanic interactions affecting the rate of dissolution of sphalerite, ECS Trans. 2 (2006) 143–153.
[29] J.L. Nava, M.T. Oropeza, I. Gonzalez, Oxidation of mineral species as a function of the anodic potential of zinc concentrate in sulfuric acid, J. Electrochem. Soc. 151 (2004) B387–B393.
[30] M. Gomez Gonzalez, O. Dominguez Renedo, M. Arcos Martinez, Speciation of antimony by adsorptive stripping voltammetry using pyrogallol, Talanta 71 (2007) 691–698.
[31] N.Y. Stozhko, O.V. Inzhevatova, L.I. Kolyadina, Determination of iron in natural and drinking waters by stripping voltammetry, J. Anal. Chem. 60 (2005) 668–672.
[32] M.A. Nolan, S.P. Kounaves, The source of the anomalous cathodic peak during ASV with in situ mercury film formation in chloride solutions, Electroanalysis 12 (2000) 96–99.
[33] D. Rahner, Fe_3O_4 as part of the passive layer on iron, Solid State Ionics 86–88 (1996) 865–871.
[34] A.F. White, M.L. Peterson, M.F. Hochella, Electrochemistry and dissolution kinetics of magnetite and ilmenite, Geochem. Cosmochim. Acta 58 (1994) 1859–1875.
[35] R.H. Lara, J. Vazquez-Arenas, G. Ramos-Sanchez, M. Galvan, L. Lartundo-Rojas, Experimental and theoretical analysis accounting for differences of pyrite and chalcopyrite oxidative behaviors for prospective environmental and bioleaching applications, J. Phys. Chem. C 119 (2015) 18364–18379.
[36] G. Gu, K. Hu, X. Zhang, X. Xiong, H. Yang, The stepwise dissolution of

chalcopyrite bioleached by Leptospirillum ferriphilum, Electrochim. Acta 103 (2013) 50–57.
[37] C.L. Liang, J.L. Xia, Y. Yang, Z.Y. Nie, X.J. Zhao, L. Zheng, C.Y. Ma, Y.D. Zhao, Characterization of the thermo-reduction process of chalcopyrite at 65 °C by cyclic voltammetry and XANES spectroscopy, Hydrometallurgy 107 (2011) 13–21.
[38] E.M. Arce, I. Gonzalez, A comparative study of electrochemical behavior of chalcopyrite, chalcocite and bornite in sulfuric acid solution, Int. J. Miner. Process. 67 (2002) 17–28.
[39] M. Eghbalnia, D.G. Dixon, Electrochemical study of leached chalcopyrite using solid paraffin-based carbon paste electrodes, Hydrometallurgy 110 (2011) 1–12.
[40] H. Zhao, J. Wang, W. Qin, M. Hu, S. Zhu, G. Qiu, Electrochemical dissolution process of chalcopyrite in the presence of mesophilic microorganisms, Miner. Eng. 71 (2015) 159–169.
[41] Y.L. Mikhlin, Y.V. Tomashevich, I.P. Asanov, A. V Okotrub, V.A. Varnek, D. V Vyalikh, Spectroscopic and electrochemical characterization of the surface layers of chalcopyrite ($CuFeS_2$) reacted in acidic solutions, Appl. Surf. Sci. 225 (2004) 395–409.
[42] F. Mansfeld, Tafel slopes and corrosion rates obtained in the pre-Tafel region of polarization curves, Corrosion Sci. 47 (2005) 3178–3186.
[43] D. Nava, I. González, Electrochemical characterization of chemical species formed during the electrochemical treatment of chalcopyrite in sulfuric acid, Electrochim. Acta 51 (2006) 5295–5303.
[44] T. das C. Almeida, E.M. Garcia, H.W.A. da Silva, T. Matencio, V. de F.C. Lins, Electrochemical study of chalcopyrite dissolution in sulfuric, nitric and hydrochloric acid solutions, Int. J. Miner. Process. 149 (2016) 25–33.
[45] S.L. Harmer, J.E. Thomas, D. Fornasiero, A.R. Gerson, The evolution of surface layers formed during chalcopyrite leaching, Geochem. Cosmochim. Acta 70 (2006) 4392–4402.
[46] Y. Li, G. Qian, J. Li, A.R. Gerson, Kinetics and roles of solution and surface species of chalcopyrite dissolution at 650 mV, Geochem. Cosmochim. Acta 161 (2015) 188–202.
[47] K. Sasaki, K. Takatsugi, K. Ishikura, T. Hirajima, Spectroscopic study on oxidative dissolution of chalcopyrite, enargite and tennantite at different pH values, Hydrometallurgy 100 (2010) 144–151.
[48] Y. Li, N. Kawashima, J. Li, A.P. Chandra, A.R. Gerson, A review of the structure, and fundamental mechanisms and kinetics of the leaching of chalcopyrite, Adv. Colloid Interface Sci. 197–198 (2013) 1–32.